

Flex-Convolution

Deep Learning Beyond Grid-Worlds

Fabian Groh^{*1}, Patrick Wieschollek^{*1,2}, and Hendrik P.A. Lensch¹

¹ University of Tübingen, ² Max Planck Institute for Intelligent Systems

Abstract. The goal of this work is to enable deep neural networks to learn representations for irregular 3D structures – just like in common approaches for 2D images. Unfortunately, current network primitives such as convolution layers are specifically designed to exploit the natural data representation of images – a fixed and regular grid structure. This represents a limitation when transferring these techniques to more unstructured data like 3D point clouds or higher dimensional data. In this work, we propose a surprisingly natural generalization *flex-convolution* of the conventional convolution layer and provide a highly efficient implementation. Compared to very specific neural network architectures for point cloud processing, our more generic approach yields competitive results on the rather small standard benchmark sets using fewer parameters and lower memory consumption. Our design even allows for *raw* neural networks prediction on several magnitudes larger point clouds, providing superior results compared to previous hand-tuned and well-engineered approaches on the 2D-3D-S dataset.

Keywords: 3D learning, point clouds, deep neural network

1 Introduction

Deep Convolutional Neural Networks (CNNs) shine on tasks where the underlying data representations are based on a regular grid structure, e.g., pixel representation of RGB images or transformed audio signals using Mel-spectrograms [1]. For these tasks, research has led to several improved neural network architectures ranging from VGG [2], Inception [3] to ResNet [4]. These architectures have established state-of-the-art results on a broad range of classical computer vision tasks and are able to process entire HD images (~ 2 million pixels) [5, 6]. This success is fueled by recent improvements in hardware and software stacks [7, 8], which provide a highly efficient implementation of layer primitives [9] in specialized libraries [10] exploiting the grid-structure of the data. Therefore, it seems appealing to also use grid-based structures (*e.g.* voxels) to process higher-dimensional data relying on these kinds of layer implementations. However, grid-based approaches are often unsuited for processing point cloud data or unstructured data.

* These two authors contributed equally.

The grid resolution on equally spaced grids poses a trade-off between discretization artifacts and memory consumption. Increasing the granularity of the cells will result in higher memory consumption that even grows exponentially due to the curse of dimensionality. While training neural networks on 3D voxel grids is possible [11], even with hierarchical octrees [12] the maximum resolution is limited to 256^3 voxels – large data sets are currently out-of-scope.

Another issue is the discretization and resampling of continuous data into a fixed grid. For example, depth sensors produce an arbitrarily oriented depth map with different resolution in x, y and z . In Structure-from-Motion, the information of images with arbitrary perspective, orientation and distance to the scene – and therefore resolution – need to be merged into a single 3D point cloud.

This potentially breaks the grid-based structure assumption completely, such that processing such data providing optimal resolution with conventional approaches is infeasible by design. These problems become even more apparent when extending current data-driven approaches to handle higher-dimensional data. A solution is to directly learn on unstructured data.

Recently, multiple attempts proposed to handle *irregular* point clouds directly in a deep neural network [13–15]. In contrast to the widely successful general purpose 2D network architectures, these methods propose very particular network architectures, which most often only are applicable for a limited range of tasks. Also, these solutions only work on rather small point clouds, they still lack support for large-scale applications. Current neural network-based approaches on the standard benchmark set ModelNet40 [16] for objects classification perform inference on instance examples with only 1024 points and the network design is limited to 4096 input points [13]. The number of points enables simple object classification, where the primary information is in the global shape characteristics. But compared to images, the point density corresponds to an image resolution of under 370 pixels for an artist-made single object vs. 784 pixels for handwritten MNIST digits. Dense 3D scenes, however, typically consist of millions of points [17, 18]. For such large-scale datasets, these methods require more specialized hand-crafted input features that already accumulate the information from larger regions [19]. For these reasons, we avoid extensive pre-processing and task-specific network designs. Our main contribution are:

1. We provide a surprisingly natural generalization of the convolution layer that paves the way for extending successfully proven and commonly used 2D network architectures to handle unstructured 3D and higher dimensional data in arbitrary metric spaces. This generalized convolution layer is memory efficient. The CUDA implementation is sufficiently fast and compares well with grid-based methods, enabling the processing of large-scale datasets.
2. We describe a neural network approach for 3D point segmentation which can handle four Million points *simultaneously* during inference. This relates to a QHD image resolution. Notably, we do not rely on any form of pre- or post-processing. The raw output of the network significantly out-performs complex hand-engineered pipelines (including post-processing enhancement steps) [18] on large-scale point cloud segmentation.

2 Related Work

Recent literature about deep learning approaches applied to more general data structures can be organized into three categories based on their way dealing with input data.

Voxel-based methods [11, 20, 21, 12] fit the unstructured 3D point cloud data into a grid of voxels to apply classical convolution layers using CNNs afterwards. However, this either loses spatial information during the discretization process or requires substantial computational resources for the 3D convolutions to avoid discretization artifacts. These approaches are affected by the curse of dimensionality and will be infeasible for higher-dimensional spaces. Interestingly, ensemble methods [22–24] based on classical CNNs still achieve state-of-the-art results on common benchmark sets like ModelNet40 [16] by rendering the 3D data from several viewing directions as image inputs. As the rendered views omit some information (*i.e.* occlusions), Cao *et al.* [25] propose to use a spherical projection.

Methods in Euclidean Space deal directly with point cloud data by trying to circumvent current hardware limitations when applying classical layer primitives. *PointNet* [13] is one of the first approaches yielding competitive results on ModelNet40 [16]. It processes each point independently using a multi-layer-perceptron and combines the information from all points using a spatial transformer module [26] in the feature space. Such a learned spatial transformer can be rather costly, in particular for higher feature dimensions. While this approach contains a rather simple architecture, it lacks the granularity of aggregating features detected in local areas only. The extension *PointNet++* [14] incorporates information from nearby points by applying “mini”-PointNets to each point neighborhood and concatenates these learned features across different resolutions. An alternative way of introducing a structure in point clouds relies on kD-trees [15], where building such an index structure allows for sharing convolution layers depending on the splitting orientation. kD-trees only allow for fusing two points each time and they are affected by the curse of dimensionality as well. Another recent approach are *Dynamic Edge-Condition Filters* [27]. The network structure learns parameters in the fashion of dynamic filter networks [28] for each single point neighborhood. Note, this requires a tremendous amount of memory to *explicitly* store a specific parameter for *each* position in *each* neighborhood, which can become quickly infeasible for reasonably large input data.

Methods for Network-Graph structures, like social networks or knowledge graphs, are particular instances of unstructured data, which can be defined inseparable from the underlying graph structure only. Hereby, the location of each node is given by its relative position to neighboring nodes. This is quite different from processing point cloud data in the Euclidean space. Recent research [29] proposes to utilize a sparse convolution for graph structures, which is based on the adjacency matrix. This effectively masks the output of intermediate values in the classical convolution layers.

3 Method

The basic operation in convolutional neural networks is a discrete convolution, where the 2D image signal¹ $I \in \mathbb{R}^{H \times W \times C}$ is convolved with a filter-kernel w . A common filter size in deep learning is $3 \times 3 \times C$ such that this mapping can be described as

$$(w \circledast f)[\ell] = \sum_{c \in C} \sum_{\tau \in \{-1, 0, 1\}^2} w_{c'}(c, \tau) f(c, \ell - \tau), \quad (1)$$

where $\tau \in \{-1, 0, 1\}^2$ describes the 8-neighborhood in regular 2D grids. One usually omits the location information as it is given implicitly by arranging the feature values in a grid. Still, each pixel information is a *pair* of a feature/pixel value $f(c, \ell)$ and its location ℓ .

In this paper we extend the convolution operation \circledast to support unstructured data with continuous data locations. In this case, the kernel w needs to support arbitrary relative positions $\ell_i - \tau_i$, which can be unbounded. Before discussing such potential versions of w , we shortly recap the grid-based convolution layer in more detail to derive desired properties of a more generic convolution operation.

3.1 Convolution Layer

For a discrete $3 \times 3 \times C$ convolution layer such a filter mapping²

$$w_{c'}: C \times \{-1, 0, 1\}^2 \rightarrow \mathbb{R}, \quad (c, \tau) \mapsto w_{c'}(c, \tau) = \sum_{\tau' \in \{-1, 0, 1\}^2} \mathbb{1}_{\{\tau = \tau'\}} w_{c, c', \tau'} \quad (2)$$

is a lookup table with 9 entries for each (c, c') pair. These values of $w_{c, c', \tau'}$ can be optimized for a specific task, *e.g.* using back-propagation when training CNNs. Typically, a single convolution layer has a filter bank of multiple filters. Note, $w_{c'}$ is neither differentiable nor continuous wrt. τ . While these lookup tables can be shared across different spatial locations ℓ , they have a bounded domain. Specifically, the 8-neighborhood in a 2D grid always has exactly the same underlying spatial layout. Hence, this approach can exploit the implicitly given locations. The same is also true for other filter sizes $k_h \times k_w \times C$.

To process unstructured data, we need to find a well-behaving function $w_{c'}$, which can handle an *unbounded* domain of arbitrary – possibly real-valued – relations between τ and ℓ , besides the ability to share parameters across different neighborhoods. To find potential candidates and identify required properties, consider a point-cloud as a more generic data representation

$$P = \{(\ell^{(i)}, f^{(i)}) \in L \times F \mid i = 0, 1, \dots, N - 1\}. \quad (3)$$

¹ $c \in C$ represents the RGB, where we abuse notation and write C for $\{0, 1, \dots, C - 1\} \subset \mathbb{N}$ as well.

² $\mathbb{1}_M$ is the indicator function being 1 iff $M \neq \emptyset$.

Besides its value $f^{(i)}$, each point cloud element now carries an *explicitly* given location information $\ell^{(i)}$. In arbitrary metric spaces, *e.g.* Euclidean space $\mathcal{M} = (\mathbb{R}^d, \|\cdot\|)$, $\ell^{(i)}$ can be real-valued and does not necessary need to lie on a discrete grid vertex.

Indeed, one way to deal with this data structure is to *voxelize* a given location $\ell \in \mathbb{R}^d$ by mapping it to a specific grid vertex, *e.g.* $L' \subset \alpha\mathbb{N}^d$, $\alpha \in \mathbb{R}$. When L' resembles a grid structure, classical convolution layers can be used after such a discretization step. As already mentioned, choosing an appropriate α causes a trade-off between rather small cells for finer granularity in L' and consequently higher memory consumption.

Instead, we propose to define the notion of a convolution operation for a set of points in a local area. For any given point at location ℓ such a set is usually created by computing the K nearest neighbor points with locations $\mathcal{N}_K(\ell) = \{\ell_0, \ell_1, \dots, \ell_{K-1}\}$ for each ℓ , *e.g.* using a kD-tree. Thus, a generalization of Eq. (1) can be written as

$$f'(c', \ell^{(i)}) = \sum_{c \in C} \sum_{\mathcal{N}_K(\ell^{(i)})} \tilde{w}(c, \ell^{(i)}, \ell_k^{(i)}) \cdot f(c, \ell_k^{(i)}). \quad (4)$$

Note, for point clouds describing an image Eq. (4) is equivalent³ to Eq. (1). But for the more general case we require that

$$\tilde{w}_{c'}: C \times \mathbb{R}^d \times \mathbb{R}^d \rightarrow \mathbb{R}, \quad (c, \ell, \ell') \mapsto \tilde{w}(c, \ell, \ell') \quad (5)$$

is an *everywhere* well-defined function instead of a simple look-up table. This ensures, we can use \tilde{w} in neighborhoods of arbitrary sizes. However, a side-effect of giving up the grid-assumption is that \tilde{w} needs to be differentiable in both ℓ, ℓ' to perform back-propagation during training. A natural choice of \tilde{w} is the scalar product between the relative location $\ell^{(i)} - \ell_k^{(i)}$ and trainable parameters θ_{ℓ_c} plus a bias term θ_{b_c} :

$$\tilde{w}(c, \ell^{(i)}, \ell_k^{(i)} | \theta_{\ell_c}, \theta_{b_c}) = \langle \theta_{\ell_c}, \ell^{(i)} - \ell_k^{(i)} \rangle + \theta_{b_c}. \quad (6)$$

It's effect is illustrated in Figure 1, which can be considered as a linear approximation of the lookup table, with the advantage of being defined everywhere. In a geometric interpretation \tilde{w} is a learnable linear transformation (scaled and rotated) of a high-dimensional Prewitt operation.

This simple extension of the grid-based convolution can represent several classical image operations like the Sobel and blur operation besides the mentioned Prewitt operator, compare Figure 2. To summarize, the linearity of \tilde{w} has several advantages:

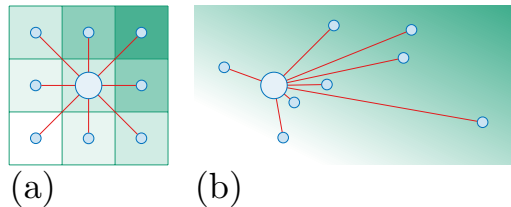


Fig. 1. A classical, discrete convolution filter (a) compared to our continuous kernel on irregular neighborhoods (Eq. (6)) in (b).

³ By setting $\mathcal{N}_9(\ell) = \{\ell - \tau | \tau \in \{-1, 0, 1\}^d\}$ and $\tilde{w}_{c'}(c, \ell^{(i)}, \ell_k^{(i)}) = w_{c'}(c, \ell^{(i)} - \ell_k^{(i)})$.

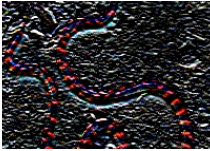
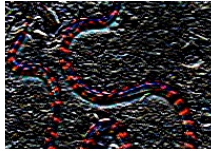




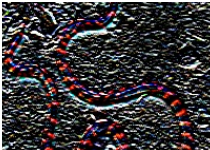
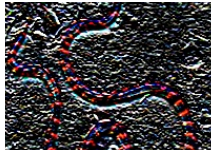

	learned	expected ($i \circledast k$)	input i	ground-truth filter k	learned parameters
Prewitt				$\begin{bmatrix} 1 & 0 & -1 \\ 1 & 0 & -1 \\ 1 & 0 & -1 \end{bmatrix}$	$\theta_x = 0.0000$ $\theta_y = 1.0058$ $\theta_b = -0.0004$
Blur				$\frac{1}{N} \begin{bmatrix} 1 & 2 & 1 \\ 2 & 4 & 2 \\ 1 & 2 & 1 \end{bmatrix}$	$\theta_x = 0.0002$ $\theta_y = -0.0022$ $\theta_b = 0.1108$
Sobel				$\frac{1}{N} \begin{bmatrix} 1 & 2 & 1 \\ 0 & 0 & 0 \\ -1 & -2 & -1 \end{bmatrix}$	$\theta_x = 0.0018$ $\theta_y = 1.3523$ $\theta_b = -0.0002$

Fig. 2. Results on a toy dataset for illustration purposes. The special-case $w(x, y) = \theta_x(x - x_0) + \theta_y(y - y_0) + \theta_{b_c}$ of Eq. (6) is trained to re-produce the results of basic image operations like Prewitt, Sobel or Blur.

1. The mapping \tilde{w} is *everywhere* well-defined in $c, \ell^{(i)}, \ell_k^{(i)}$. Hence, it can cover different distance ranges of neighborhood entries without the need for discretization or value clipping.
2. The trainable parameters θ_c, θ_{b_c} can be shared across different neighborhoods in different spatial locations like in the classical grid-based version. Hence, \tilde{w} is translation invariant and the required memory consumption for storing parameters is small.
3. The mapping \tilde{w} is continuous differentiable wrt. to *all* arguments, such that gradients can be propagated back even through the location $\ell^{(i)}, \ell_k^{(i)}$.
4. This operation can be efficiently implemented using CUDA to benefit from the sparse access patterns of local neighborhoods. Consequently, this drastically reduces the memory footprint, which is crucial when applying this method to large-scale settings.

Compared to previous methods, this formulation overall results in a significant reduction of the required network parameters.

3.2 Sub-Sampling

While straight-forward in grid-based methods, a proper and scalable sub-sampling operation in unstructured data is not canonically defined. On grids down-sampling the input by a factor 4 is usually done by simply taking every second cell in each dimension and aggregating the corresponding information, see Figure 3 (a). There is always an implicitly well defined connection between a point and its representative at a coarser resolution.

For sparse structures this property no longer holds. Points being neighbors in one resolution, potentially are not in each other’s neighborhood at a finer resolution. Hence, it is even possible that some points will have no representative within the next coarser level.

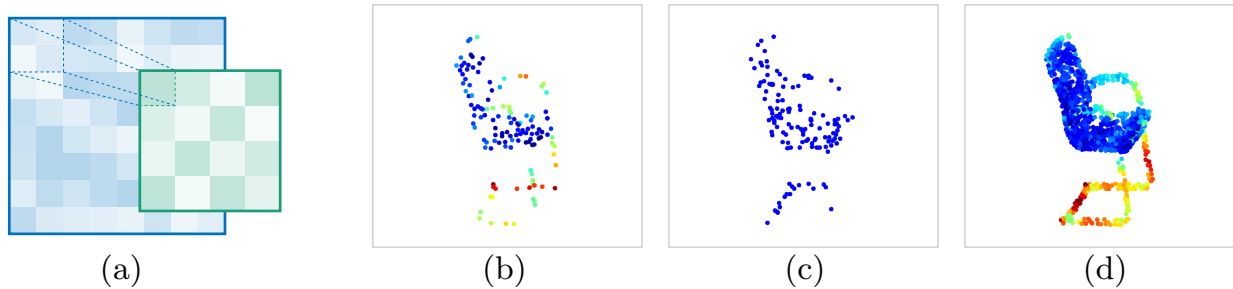


Fig. 3. Comparing strided sub-sampling in (a) regular grids and inverse density importance sub-sampling (IDISS) (b) against random sub-sampling (c) for an object (d). Note, how the chair legs are rarely existing in a randomly sub-sampled version, while IDISS preserves the overall structure.

To avoid this issue, Simonovsky *et al.* [27] uses the VoxelGrid algorithm which inherits all voxel-based drawbacks described in the previous chapter. Qi *et al.* [14] utilizes Farthest point sampling (FPS). While this produces sub-samplings avoiding the missing representative issue, it pays the price of having the complexity of $\mathcal{O}(N^2)$ for *each* down-sampling layer. This represents a serious computation limitation. Instead, we propose to utilize inverse density importance sub-sampling (IDISS). In our approach, the inverse density ϕ is simply approximated by adding up all distances from one point in ℓ to its K -neighbors:

$$\phi(\ell) = \sum_{\mathcal{N}_K(\ell)} \|\ell - \ell_k\|. \quad (7)$$

Sampling the point cloud proportional to this distribution has a computational complexity of $\mathcal{O}(N)$, and thereby enables processing million of points in a very efficient way. In most cases, this method is especially cheap regarding computation time, since the distances have already been computed to find the K -nearest neighbors. Compared to pure random sampling, it produces better uniformly distributed points at a coarser resolution and more likely preserves important areas. In addition, it still includes randomness that is preferred in training of deep neural networks to better prevent against over-fitting.

4 Implementation

To enable building complete DNNs with the presented flex-convolution model we have implemented two specific layers in TensorFlow [7]: *flex-convolution* and *flex-max-pooling*. Profiling shows that a direct implementation in CUDA leads to a run-time which is in the range of regular convolution layers during inference.

4.1 Neighborhood Processing

Both new layers require a known neighborhood for each incoming point. For a fixed set of points this neighborhood is computed once upfront based on an efficient kD-tree implementation and kept fixed. For each point the K nearest neighbors are stored as indices into the point list. The set of indices is represented as a tensor and handed over to each layer.

The *flex-convolution* layer merely implements the convolution with continuous locations as described in Eq. (6). Access to the neighbors follows the neighbor indices to lookup their specific feature vectors and location. No data duplication is necessary. As all points have exactly the same number of neighbors this step can be parallelized very efficiently. In order to make the position of each point available in each layer of the network we attach the point location ℓ to each feature vector.

The *flex-max-pooling* layer implements max-pooling over each point neighborhood individually. As long as the point set stays the same the same neighborhood indices are valid.

For subsampling we exploit the IDISS approach described in Section 3.2. Flex-max-pooling is applied to each selected point with the current neighborhood to down-sample and filter the features from the previous larger-sized layer. For the subsequent, subsampled layers a new neighborhood is computed which only includes the subsampled points.

Upsampling (flex-max-unpooling) is done by copying the features of the selected points into the larger-sized layer, initializing all other points with zero, like zero-padding in images and performing the flex-max-pooling operation.

4.2 Efficient Implementation of Layer Primitives

To ensure a reasonably fast training time, highly efficient implementations of flex-convolution and flex-max-pooling as a custom operation in TensorFlow using CUDA are required. We compare our optimized CUDA kernel against a pure version containing exclusively existing operations provided by the TensorFlow framework itself and its grid-base counterpart in cuDNN [10].

Table 1 provides the information from the CUDA profiler for a *single* flex-convolution layer on a set of parameters, which fits typical hardware (Nvidia GTX 1080Ti). As the grid-based convolution layer typically uses a kernel-size of $3 \times 3 \times C$, we set $k = 9$ as well – though we use $k = 8$ in all subsequent experiments. We did some experiments with a quite recent polyhedral compiler optimization using TensorComprehension (TC) [30] to automatically tune a flex-convolution layer implementation. While this approach seems promising and provides further speedup, the lack of supporting flexible input sizes currently prevents us from using these automatically generated CUDA kernels in practice.

An implementation of the flex-convolution layer by just relying on operations provided by the TensorFlow framework requires data duplication. We had to spread the pure TensorFlow version across 8 GPUs to run a *single* flex-convolution layer. Typical networks usually consist of several such operations.

Table 1. Profiling information of diverse implementations of Eq. (6) and its gradients using a CUDA profiler. These benchmarks process a batch of $b = 8$ elements each with 4096 points. We use neighborhood size $k = 9$ and feature dimensions $C' = C = 64$. Runs marked with (*) were spread across multiple GPUs to fit into GPU memory.

Method	Timing		Memory	
	Forward	Backward	Forward	Backward
flex-convolution (pure TF)*	1829ms	2738ms	34015.2MB	63270.8MB
flex-convolution (generic)	67ms	265ms	8.4MB	8.7MB
flex-convolution (TC [30])	42ms	-	8.4MB	-
grid-based conv.($3 \times 3 \times 64$)	16ms	1.5ms	1574.1MB	153.4MB
flex-max-pooling (generic)	1.44ms	15us	16.78MB	8.4MB

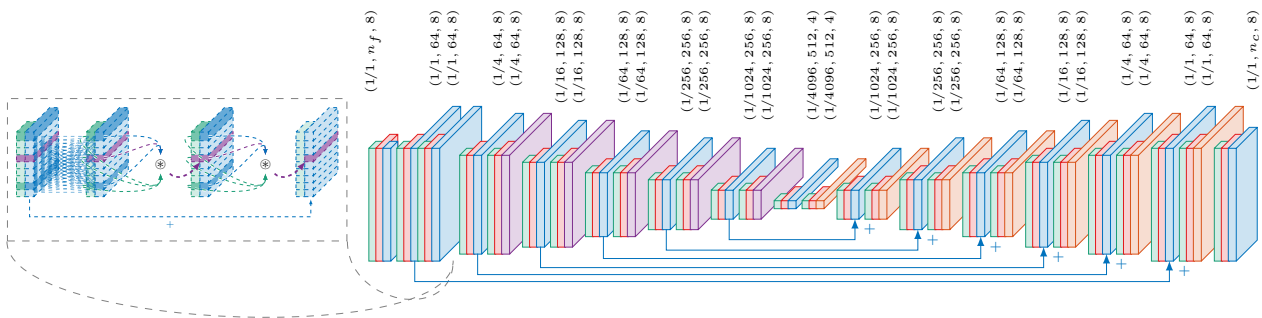


Fig. 4. Network architecture for semantic 3D point cloud segmentation. The annotations (a, d_f, k) represent the spatial resolution factor a (*i.e.* using $a \cdot n$ points) and feature length d_f with n_f input features and n_c classes. The used neighborhood size is given by k . In each step, the position information \blacksquare and neighborhood information \blacksquare is required besides the actual learned features. After flex-convolution layers \blacksquare , each downsampling step \blacksquare (flex-max-pool) has a skip-connection to the corresponding decoder block with flex-max-unpooling layer \blacksquare .

Hence, it is inevitable to recourse on tuning custom operation when applying such a technique to larger datasets.

4.3 Network Architecture

With the new layers we can directly transfer the structure of existing image processing networks to the task of processing large point clouds. We will elaborate on our network design and choice of parameters for the task of semantic point-cloud segmentation in more detail. Here, we draw inspiration from established hyper-parameter choices in 2D image processing.

Our network architecture follows the SegNet-Basic network [31] (a 2D counterpart for semantic image segmentation) with additional Unet-skip-connections [32]. It has a typical encoder-decoder network structure followed by a final point-wise soft-max classification layer. To not obscure the effect of the flex-convolution layer behind several other effects, we explicitly do *not* use tricks like

Batch-Normalization, weighted soft-max classification, or computational expensive pre/post-processing pipelines, which are known to enhance the prediction quality and could further be applied to the results presented in the Section 5.

The used architecture and output sizes are given in Figure 4. The encoder network is divided into six stages of different spatial resolutions to process multi-scale information from the input point cloud. Each resolution stage consists of two ResNet-blocks. Such a ResNet block chains the following operations: 1×1 -convolution, flex-convolution, flex-convolution (compare Figure 4). Herewith, the output of the last flex-convolution layer is added to the incoming feature following the common practice of Residual Networks [4]. To decrease the point-cloud resolution across different stages, we add a flex-max-pooling operation as the final layer in each stage of the encoder. While a max-pooling of images is normally done with stride 2 in each image dimension, we use the flex-max-pooling layer to reduce the resolution by factor 4. When the spatial resolution decreases, we increase the feature-length by factor two.

Moreover, we experimented with different neighborhood sizes k for the flex-convolution layers. Due to speed considerations and the widespread adoption of 3×3 filter kernels in image processing we stick to a maximal nearest neighborhood size of $k = 8$ in all flex-convolution layers. We observed no decrease in accuracy against choosing $k = 16$ but a drop in speed by factor 2.2.

The decoder network mirrors the encoder architecture. We add skip connections [32] from each stage in the encoder to its related layer in the decoder. Increasing spatial resolution at the end of each stage is done via flex-max-unpooling. We tested a trainable flex-deconvolution layer in some preliminary experiments and observed no significant improvements. As flex-max-unpooling is more light-weight (see Table 1) regarding computation effort, we preferred this operation. As this is the first network being able to process point clouds in a large-scale setting, we expect choosing more appropriate hyper-parameters is possible when investing more computation time.

5 Experiments

We provide several experiments to validate our approach. We show that our flex-convolution-based neural network yields competitive performance to previous work on the ModelNet40 [16] dataset using fewer resources and provide some insights about human performance on this dataset. We visualize learned features by computing saliency maps of the input. Furthermore, we demonstrate the effectiveness of our approach by performing semantic point cloud segmentation on the large-scale 2D-3D-S dataset [18] significantly out-performing previous methods. The properties of the used datasets are given in Table 2.

5.1 ModelNet40

The ModelNet40 [16] dataset consists of 40 categories of 3D models, each containing variations of objects created by digital artists. The models are represented

Table 2. Properties of used datasets during this evaluation. While the ModelNet40 contains relatively simple models created by artist, the Stanford 2D-3D-S dataset contains information from a real-world 3D scanning of a real building complex.

Dataset	#Classes	#Points	Source	Task
ModelNet [16]	40	$20 \cdot 10^6$ 1024	human made per object	object classification during inference
2D-3D-S [18]	14	$27 \cdot 10^7$	3D scanning	semantic segmentation

by 3D point sets randomly sampled on the surface. We applied a smaller version of the previously described encoder network-part followed by a fully-connected layer and a classification layer.

During evaluation, we use the official test-split [13] and follow the common evaluation protocol for object classification by random sampling 1024 points for each object in a batch during training. Table 3 lists the performance of different approaches in object classification using ModelNet40. Notably, in contrast to both PointNet versions [13, 14] we do *not* need to train a specialized spatial transformer module, or augment the input by applying different rotations — we just follow a typical pipeline from 2D image classification. Further, our predictions are provided from by a single forward-pass in contrast to

a voting procedure as in the KD-Net approach [15]. This demonstrates, that a small flex-convolution neural network with significant fewer parameters provides competitive results on this benchmark set. Even when using just 1/4th of the point-cloud and thus an even smaller network the accuracy remains competitive.

To put these values in a context to human perception, we conducted a user study. Each participant was asked to classify point clouds sampled from the official test split. We allowed them to rotate the presented point cloud for the task of classification without a time limit. Averaging all 2682 gathered object classification votes from humans reveals some difficulties with this dataset. This might be related to relatively unconventional choice of categories in the dataset, *i.e.* plants and their flower pots and bowls are sometimes impossible to separate. Please refer to the Supplementary for a screenshot of the used interface along with a confusion matrix.

To investigate possible traits the network is looking for, we computed saliency maps, see Figure 5. These suggest that the network is focusing on segment-joints like the junction between the seating surface and the leg of the chair as well as identifying typical object contours in the case of sofa and table. These

Table 3. Classification accuracy on ModelNet40 (1024 points) and 256 points*.

Method	Accuracy	#params.
PointNet [13]	89.2	1'622'705
PointNet2 [14]	90.7	1'658'120
KD-Net[15]	90.6	4'741'960
D-FilterNet [27]	87.4	345'288
Human	64.0	-
Ours	90.2	346'409
Ours* (1/4)	89.3	171'048

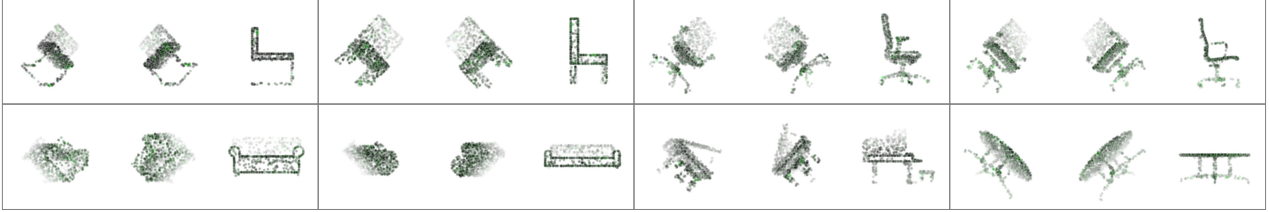


Fig. 5. Saliency maps of test objects in ModelNet40 reconstructed by our classification network from different perspectives. The highlighted regions have strong influence on the produced outputs. The network is clearly looking for joints between different object segments and typical object outlines.

observations hold for all object of the same class as illustrated in the top row of Figure 5.

5.2 Semantic Point-Cloud Segmentation

Another common computer vision task is semantic segmentation, which splits a given input into distinct smaller units. To test the scalability of our approach, we applied the described network from Section 4.3 to the 2D-3D-S dataset [18]. This real-world dataset covers 3D scanning information from six square kilometers of several building complexes collected by a Matterport Camera [33].

The dataset comes along with several information like equirectangular images with depth maps, RGB images, 3D meshes and surface normals. Previous approaches [19, 18] build a voxel-based sliding window approach, which utilizes these information besides additional hand-crafted feature, *e.g.* local curvature, occupancy and point density information per voxel. We argue, that a neural network as described in Section 4.3 can learn all necessary features directly from the data – just like in the 2D case. In our approach, we skip all pre-processing steps proposed by Armeni *et al.* [18] and just provide the neural network with normalized position information x, y, z and RGB information per point. Our ablation study (see Table 4) suggest, that even using constant initial features besides the neighborhood indices already provides enough information to successfully perform semantic segmentation. To account for the irregularity in the data, it is however useful to use normalized position data besides the color information from the 2D case. Previous approaches solve an *integer-program* in an energy-based maximization problem (S-SVM-CRF) [34] to enforce contextual consistency. Instead, our *fully-convolutional* approach only contains a single forward pass for each room during inference, followed by a cheap mean filter in each K -neighborhood. Results could further be boosted by CRF-base post-processing in the future. Following the official evaluation protocol, it is noteworthy that our raw network predictions significantly out-performs

Table 4. Ablation study on the effect of different input features in a typical room.

Input Feature	mAP
Constant	0.31
Position	0.39
Position, RGB	0.50

Table 5. Class specific average precision (AP) on the 2D-3D-S dataset. The approach in [18] is not network-based but applies a linear classifier, integer programming and CRFs. (\ddagger) uses additional input features like local curvature, point densities, surface normals. (*) uses an CRF-based post-processing and (**) a mean filter post-processing.

	Moveable Elements						Structural Elements								Overall
	Table	Chair	Sofa	Bookcase	Board	Mean	Ceiling	Floor	Wall	Beam	Column	Window	Door	Mean	Mean
[18]*	46.02	16.15	6.78	54.71	3.91	25.51	71.61	88.70	72.86	66.67	91.77	25.92	54.11	67.38	49.93
[18]* \ddagger	39.87	11.43	4.91	57.76	3.73	23.78	50.74	80.48	65.59	68.53	85.08	21.17	45.39	58.73	44.19
Ours	66.03	51.75	15.59	39.03	43.50	43.18	87.20	96.00	65.53	54.76	52.74	55.34	35.81	63.91	55.27
Ours**	67.02	52.75	16.61	39.26	47.68	44.66	87.33	96.10	65.52	56.83	55.10	57.66	36.76	65.04	56.55

previous approaches given the same available information and approaches using additional input information, see Table 5. While significantly improving state-of-the-art results on 2D-3D-S [18] our network lacks precision in categories like beam, column and door. Providing features like local curvature besides post-processing [18] greatly simplify detecting these kind of objects.

Consider Figure 6, the highlighted window region in room A is classified as wall because the blinds are closed having similar appearance. In room B, our network miss-classifies the highlighted column as “wall”, which is not surprising as both share similar geometry and color. Interestingly, in room C our network classifies the beanbag as “sofa”, while its ground-truth annotation is “chair”.

Training is done on two Nvidia GTX 1080Ti GPUs with a total batch-size 16 for two days for each k -fold split. Each batch entry contains a randomly selected sub point-cloud chunk with $n = 128^2$ points. We found no significant differences between different learning rates, so we stick with the defaults of the Adam-Optimizer and a learning-rate of $3 \cdot 10^{-3}$.

6 Conclusion

For unstructured point sets our work demonstrates for the first time an effective natural extension to the traditional convolution, transposed convolutions and max-pooling primitives which scale well even for large data sets.

The layers operate on the local neighborhood of each point, which is provided by indices to the K nearest neighbors. Compared to 3D CNNs our approach easily supports even high-dimensional point sets.

As the introduced layers behave very similar to convolution layers in networks designed for 2D image processing we can leverage the full potential of already successful architectures. This is against recent trends in point cloud processing with highly specialized architectures which sometimes rely on hand-crafted input features, or heavy pre- and post-processing. We demonstrate state-of-the-art classification and segmentation results while at the same time allowing for simultaneous processing of million of points.

With the advent of automated CUDA kernel tuning (TensorComprehension) [30] we believe that processing point clouds will gain further speed up, getting even closer to cuDNN [10] for both learning and inference.

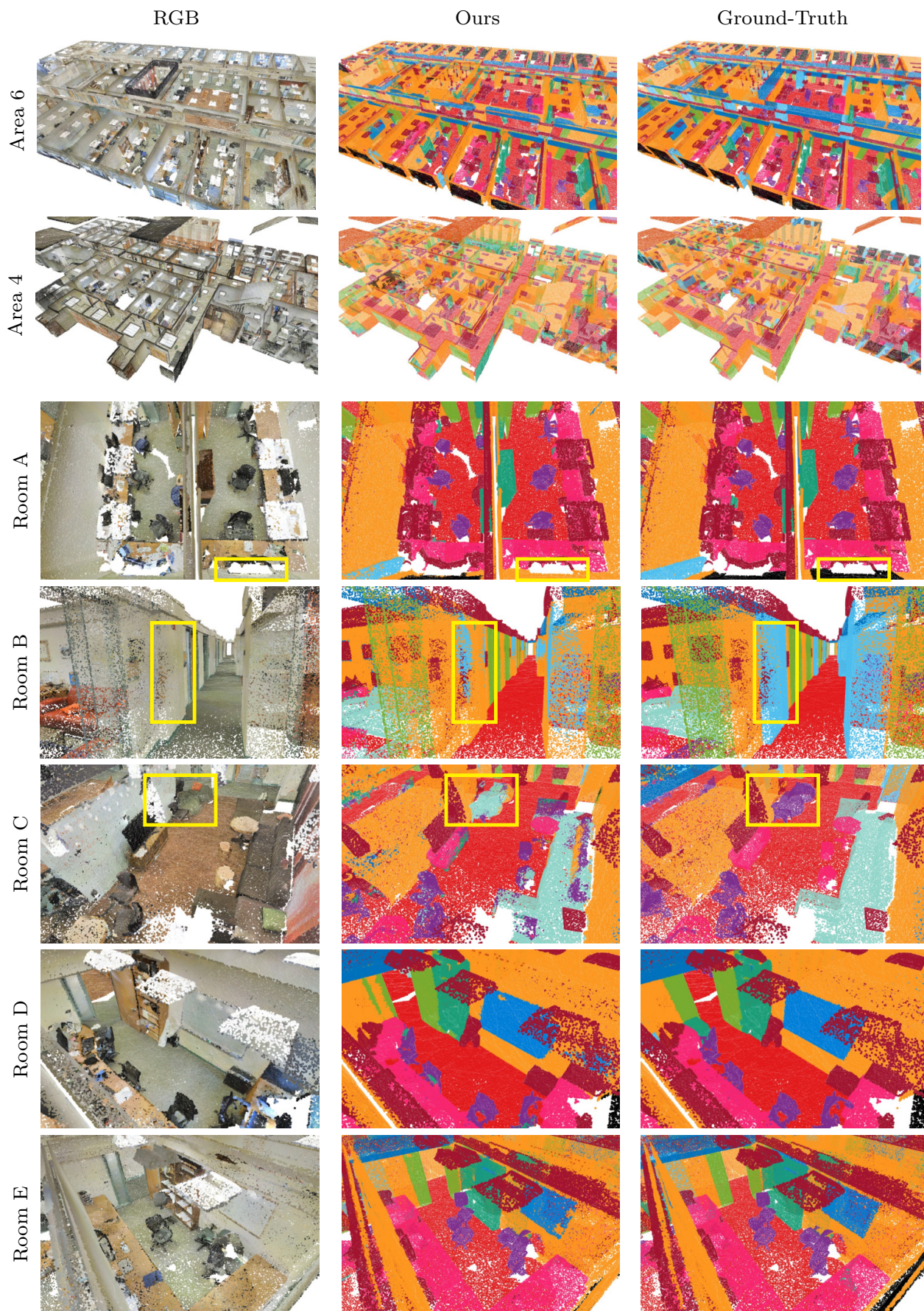


Fig. 6. Semantic point cloud segmentation produced as raw outputs of our proposed network from the held-out validation set. In this point-based rendering, surfaces might not be illustrated as opaque.

References

1. Hershey, S., Chaudhuri, S., Ellis, D.P.W., Gemmeke, J.F., Jansen, A., Moore, C., Plakal, M., Platt, D., Saurous, R.A., Seybold, B., Slaney, M., Weiss, R., Wilson, K.: Cnn architectures for large-scale audio classification. In: IEEE International Conference on Acoustics, Speech and Signal Processing (ICASSP). (2017)
2. Simonyan, K., Zisserman, A.: Very deep convolutional networks for large-scale image recognition. CoRR (2014)
3. Szegedy, C., Liu, W., Jia, Y., Sermanet, P., Reed, S., Anguelov, D., Erhan, D., Vanhoucke, V., Rabinovich, A.: Going deeper with convolutions. In: Proceedings of the IEEE Conference on Computer Vision and Pattern Recognition (CVPR). (2015)
4. He, K., Zhang, X., Ren, S., Sun, J.: Identity mappings in deep residual networks. In: Proceedings of the European Conference on Computer Vision (ECCV). (2016) 630–645
5. Wieschollek, P., Schölkopf, M.H.B., Lensch, H.P.A.: Learning blind motion deblurring. In: Proceedings of the IEEE International Conference on Computer Vision (ICCV). (October 2017)
6. Sajjadi, M.S.M., Schölkopf, B., Hirsch, M.: EnhanceNet: Single image super-resolution through automated texture synthesis. In: Proceedings of the IEEE International Conference on Computer Vision (ICCV). (2017)
7. Abadi, M., Agarwal, A., Barham, P., Brevdo, E., Chen, Z., Citro, C., Corrado, G.S., Davis, A., Dean, J., Devin, M., Ghemawat, S., Goodfellow, I., Harp, A., Irving, G., Isard, M., Jia, Y., Jozefowicz, R., Kaiser, L., Kudlur, M., Levenberg, J., Mané, D., Monga, R., Moore, S., Murray, D., Olah, C., Schuster, M., Shlens, J., Steiner, B., Sutskever, I., Talwar, K., Tucker, P., Vanhoucke, V., Vasudevan, V., Viégas, F., Vinyals, O., Warden, P., Wattenberg, M., Wicke, M., Yu, Y., Zheng, X.: TensorFlow: Large-scale machine learning on heterogeneous systems (2015) Software available from tensorflow.org.
8. Community, P.: Pytorch. <http://pytorch.org/> (2017)
9. Lavin, A., Gray, S.: Fast algorithms for convolutional neural networks. In: Proceedings of the IEEE Conference on Computer Vision and Pattern Recognition (CVPR). (2016) 4013–4021
10. Chetlur, S., Woolley, C., Vandermersch, P., Cohen, J., Tran, J., Catanzaro, B., Shelhamer, E.: cudnn: Efficient primitives for deep learning. CoRR (2014)
11. Maturana, D., Scherer, S.: VoxNet: A 3D Convolutional Neural Network for Real-Time Object Recognition. In: IROS. (2015)
12. Riegler, G., Ulusoy, A.O., Bischof, H., Geiger, A.: Octnetfusion: Learning depth fusion from data. In: International Conference on 3D Vision (3DV) 2017. (October 2017)
13. Qi, C.R., Su, H., Mo, K., Guibas, L.J.: Pointnet: Deep learning on point sets for 3d classification and segmentation. Proceedings of the IEEE Conference on Computer Vision and Pattern Recognition (CVPR) (2017)
14. Qi, C.R., Yi, L., Su, H., Guibas, L.J.: Pointnet++: Deep hierarchical feature learning on point sets in a metric space. In Guyon, I., Luxburg, U.V., Bengio, S., Wallach, H., Fergus, R., Vishwanathan, S., Garnett, R., eds.: Advances in Neural Information Processing Systems 30. Curran Associates, Inc. (2017) 5099–5108
15. Klokov, R., Lempitsky, V.: Escape from cells: Deep kd-networks for the recognition of 3d point cloud models. In: Proceedings of the IEEE International Conference on Computer Vision (ICCV). (10 2017) 863–872

16. Wu, Z., Song, S., Khosla, A., Yu, F., Zhang, L., Tang, X., Xiao, J.: 3d shapenets: A deep representation for volumetric shapes. In: Proceedings of the IEEE Conference on Computer Vision and Pattern Recognition (CVPR). (2015) 1912–1920
17. Lian, Z., Zhang, J., Choi, S., ElNaghy, H., El-Sana, J., Furuya, T., Giachetti, A., Guler, R.A., Lai, L., Li, C., Li, H., Limberger, F.A., Martin, R., Nakanishi, R.U., Neto, A.P., Nonato, L.G., Ohbuchi, R., Pevzner, K., Pickup, D., Rosin, P., Sharf, A., Sun, L., Sun, X., Tari, S., Unal, G., Wilson, R.C.: Non-rigid 3D Shape Retrieval. In Pratikakis, I., Spagnuolo, M., Theoharis, T., Gool, L.V., Veltkamp, R., eds.: Eurographics Workshop on 3D Object Retrieval, The Eurographics Association (2015)
18. Armeni, I., Sener, O., Zamir, A.R., Jiang, H., Brilakis, I., Fischer, M., Savarese, S.: 3d semantic parsing of large-scale indoor spaces. In: Proceedings of the IEEE Conference on Computer Vision and Pattern Recognition (CVPR). (2016)
19. Armeni, I., Sax, A., Zamir, A.R., Savarese, S.: Joint 2D-3D-Semantic Data for Indoor Scene Understanding. ArXiv e-prints (February 2017)
20. Qi, C.R., Su, H., Niessner, M., Dai, A., Yan, M., Guibas, L.J.: Volumetric and multi-view cnns for object classification on 3d data. Proceedings of the IEEE Conference on Computer Vision and Pattern Recognition (CVPR) (2016)
21. Wu, Z., Song, S., Khosla, A., Yu, F., Zhang, L., Tang, X., Xiao, J.: 3d shapenets: A deep representation for volumetric shapes. In: Proceedings of the IEEE Conference on Computer Vision and Pattern Recognition (CVPR). (2015)
22. Su, H., Maji, S., Kalogerakis, E., Learned-Miller, E.G.: Multi-view convolutional neural networks for 3d shape recognition. CoRR (2015)
23. Sfikas, K., Pratikakis, I., Theoharis, T.: Ensemble of panorama-based convolutional neural networks for 3d model classification and retrieval. Computers and Graphics (2017)
24. Brock, A., Lim, T., Ritchie, J.M., Weston, N.: Generative and discriminative voxel modeling with convolutional neural networks. CoRR (2016)
25. Cao, Z., Huang, Q., Ramani, K.: 3d object classification via spherical projections. (12 2017)
26. Jaderberg, M., Simonyan, K., Zisserman, A., kavukcuoglu, k.: Spatial transformer networks. In Cortes, C., Lawrence, N.D., Lee, D.D., Sugiyama, M., Garnett, R., eds.: Advances in Neural Information Processing Systems (NIPS). Curran Associates, Inc. (2015) 2017–2025
27. Simonovsky, M., Komodakis, N.: Dynamic edge-conditioned filters in convolutional neural networks on graphs. In: Proceedings of the IEEE Conference on Computer Vision and Pattern Recognition (CVPR). (2017)
28. De Brabandere, B., Jia, X., Tuytelaars, T., Van Gool, L.: Dynamic filter networks. In: Advances in Neural Information Processing Systems (NIPS). (2016)
29. Kipf, T.N., Welling, M.: Semi-supervised classification with graph convolutional networks. In: International Conference on Learning Representations (ICLR). (2017)
30. Vasilache, N., Zinenko, O., Theodoridis, T., Goyal, P., DeVito, Z., Moses, W.S., Verdoolaege, S., Adams, A., Cohen, A.: Tensor comprehensions: Framework-agnostic high-performance machine learning abstractions (2018)
31. Badrinarayanan, V., Kendall, A., Cipolla, R.: Segnet: A deep convolutional encoder-decoder architecture for image segmentation. IEEE Transactions on Pattern Analysis and Machine Intelligence (2017)
32. Ronneberger, O., P.Fischer, Brox, T.: U-net: Convolutional networks for biomedical image segmentation. In: Medical Image Computing and Computer-Assisted

Intervention (MICCAI). Volume 9351 of LNCS., Springer (2015) 234–241 (available on arXiv:1505.04597 [cs.CV]).

33. Matterport: 3d models of interior spaces. <http://matterport.com/> (2017)
34. Koppula, H.S., Saxena, A.: Anticipating human activities using object affordances for reactive robotic response. *IEEE Transactions on Pattern Analysis and Machine Intelligence (PAMI)* **38**(1) (January 2016) 14–29